Implementation of scatter corrected List-Mode OP-EM reconstruction algorithm and a dual (Histogram/List-Mode) reconstruction scheme for dynamic PET imaging

Ju-Chieh (Kevin) Cheng, Arman Rahmim, *Member, IEEE,* Stephan Blinder, Marie-Laure Camborde, and Vesna Sossi, *Member, IEEE*

***Abstract*– We describe an implementation of Ordinary Poisson List-Mode Expectation Maximization (OP-LMEM) algorithm for the High Resolution Research Tomography (HRRT) with a scatter correction method based on the Single Scatter Simulation (SSS) technique, and a random correction method based on the variance-reduced delayed-coincidence technique. A hybrid EM algorithm has also been implemented in list-mode reconstruction (H-LMEM) using delayed-coincidence event subtraction technique with the same scatter correction as in OP-LMEM. The reconstructed images of a dynamic scanning sequence of a contrast phantom have been compared with those reconstructed using the histogram-mode reconstruction, in particular, 3D Ordinary Poisson Ordered Subset Expectation Maximization (3D-OP) with the same variance-reduced random and estimated scatter. The transaxial and axial profile analyses have shown excellent agreement between histogram and both list-mode reconstructions. Likewise the preliminary contrast and noise analyses have shown a close agreement between histogram-mode and both list-mode reconstructions. Based on these results, a dual reconstruction scheme can now be applied to dynamic imaging in Positron Emission Tomography (PET) with scatter correction; i.e. histogram-mode reconstruction (3D-OP) can be applied to frames with a large number of counts, and list-mode reconstruction (OP-LMEM) will subsequently be used for low statistics frames, as an effort to obtain efficient and quantitatively accurate reconstructions applicable to state-of-the-art dynamic PET imaging using the HRRT.**

I. Introduction

LIST-mode reconstruction for PET imaging has been established to be advantageous for low statistics studies where data are reconstructed on an event basis thus rendering the reconstruction time proportional to the number of acquired events [1]. In contrast, conventional histogram-mode reconstruction has a fixed time cost for every frame since data are reconstructed on a line-of-response (LOR) basis. Histogram-mode reconstruction is thus time-wise more efficient for high statistics studies. As a result, especially in a dynamic study, it would be advantageous to have the ability to choose the time-wise optimal reconstruction mode for each frame on the basis of the number of events acquired during that time frame.

Until recently no practical scatter correction was implemented for list-mode based reconstruction. In this study we present a modified Ordinary Poisson List-Mode Expectation Maximization algorithm (OP-LMEM) [2] that includes a scatter correction based on a Single Scatter Simulation (SSS) [3]. The implementation of this algorithm is discussed together with a comparison of images reconstructed with the corresponding sinogram based algorithm (i.e. 3D Ordinary Poisson Ordered Subset Expectation Maximization (3D-OP)) [4]. In addition, a hybrid EM algorithm has also been implemented into the list-mode reconstruction with the same scatter estimate as OP-LMEM while using a direct random subtraction approach with image based non-negativity constraint [1] to investigate the effect of the variance reduced random estimate.

II. Ordinary Poisson EM in List-Mode Reconstruction

In subsetized histogram-mode reconstruction, data acquired are divided into angular subsets in order to speed up the convergence of the reconstruction and reduce the number of iterations required. Similarly, in subsetized list-mode reconstruction, data acquired for a frame in the dynamic studies are divided into "segmented time subsets" (i.e. time subsets are regrouped from the subset segments as shown in Fig.1 to minimize the inconsistencies between the activity distributions for the sequential time subsets thus characterizing the average activity distribution within the time frame) [2], and the image of the dynamic frame is updated after processing through each subset.

Manuscript received November 10, 2005. This work was supported by the Canadian Institute of Health Research, the TRIUMF Life Science grant, the Natural Sciences and Engineering Research Council of Canada UFA (V. Sossi), and the Michael Smith Foundation for Health Research scholarship (V. Sossi).

J.-C. Cheng and V. Sossi are with the Department of Physics and Astronomy, University of British Columbia, Vancouver, BC V6T 1Z1 (e-mail jcheng@phas.ubc.ca, vesna@phas.ubc.ca).

A. Rahmim was with the Department of Physics and Astronomy, University of British Columbia, Vancouver, BC V6T 1Z1. He is now with the Department of Radiology, Johns Hopkins University School of Medicine, Baltimore, MD 21205 (e-mail arahmim1@jhmi.edu).

S. Blinder and M-L. Camborde are with the Pacific Parkinson's Research Centre, Vancouver, BC, V6T 1Z1 (e-mail blinder@phas.ubc.ca, marie@pet.ubc.ca).

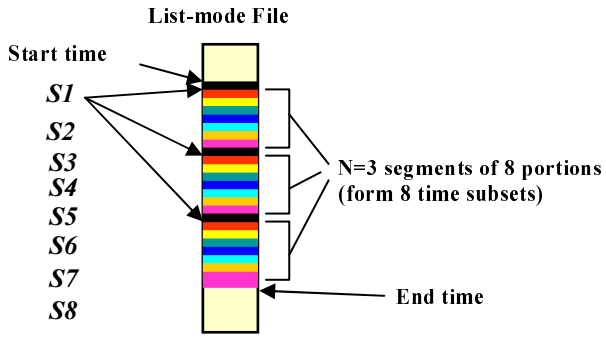

Fig.1. A dynamic frame is divided into a number of subset segments, the segments are further divided into 8 portions, and the first list-mode time subset is formed by regroup the first of the 8 portions from the segments; the number of segments is equal to 3 in this example.

The subsetized Ordinary Poisson List-Mode Expectation Maximization (OP-LMEM) algorithm is given by:

$$\lambda_j^{m,l+1} = \frac{\lambda_j^{m,l}}{\sum_{i=1}^{I} w_{ii} p_{ij}} \sum_{k=1}^{N} p_{ikj} \frac{1}{\sum_{b=1}^{J} p_{ikb} \lambda_b^{m,l} + [\bar{r}_{ik} + \bar{s}_{ik}] / w_{ii}} \quad (1)$$

where $\bar{s}_{ik}$ is the expected mean scatter counts along the i_k th LOR associated with the k th event (k = 1,……, N where N is the total number of events). $\bar{r}_{ik}$ is the expected mean random counts along the i_k th LOR associated with the k th event. $\lambda_j^{m,l}$ is the image intensity (counts) in voxel j (j = 1,……, J) at the m th iteration and l th subset. P_{ij} is the probability of an emission from voxel j being detected along the i th LOR. W_{ii} is the weight, assigned to each LOR, which accounts for sensitivity variations due to attenuation and normalization. The expected random estimate used in the OP-LMEM is computed and histogramed into a random sinogram on a frame by frame basis. It is based on the variance reduced delay coincidence technique in which crystal singles rates are estimated from the delayed-coincidence measurements (inherently including the effect of dead time), and then an iterative calculation of randoms rates is performed from the singles rate per crystal [5]-[7]. The expected scatter estimate used in the OP-LMEM algorithm here is based on a Single Scatter Simulation technique (SSS) in which the scatter contributions are calculated and histogramed into a scatter sinogram on a frame by frame basis [3]. This approach requires an intermediate histogramming step in the list-mode reconstruction to obtain the scatter and random estimate. Instead of estimating the scatter and random on a subset by subset basis in which the statistics is low (i.e. poor scatter and random estimate) and the time cost is proportional to the number of subsets, a scatter and smoothed random sinogram is estimated for each frame. In the OP-LMEM, the estimated scatter and random events are then distributed or scaled amongst the time subsets taking into account of dead time and decay issues. In addition, the list-mode data have been aligned to the closest LOR in span 3 in order to use the span 3 scatter and random estimates.

In order to speed up the convergence of OP-LMEM the scatter and random estimates are introduced into the image update factor starting with the second subset. It was in-fact found that the image estimate "updates" itself much more quickly in the denominator of the OP-LMEM algorithm without the scatter and random estimates in the first time subset of the first iteration. The image estimate obtained from the first subset (similar to a sinogram-subtraction precorrection based algorithm), will thus be more quantitatively commensurate with respect to the expected scatter and random estimates if obtained without the inclusion of the scatter and random estimates (i.e. less magnitude difference between the image, scatter, and random estimates).

III. Hybrid EM Reconstruction Using Delayed Events Subtraction Technique

A hybrid EM algorithm has also been implemented into the list-mode reconstruction. Here the same scatter estimate is used as in the OP-LMEM algorithm, and the delayed events subtraction technique is used for the random correction thus reducing the time cost of computing the variance reduced random estimate.

$$\lambda_j^{m,l+1} = \frac{\lambda_j^{m,l}}{\sum_{i=1}^{I} w_{ii} p_{ij}} \sum_{k=1}^{N} p_{ikj} \frac{\delta_k}{\sum_{b=1}^{J} p_{ikb} \lambda_b^{m,l} + [\bar{s}_{ik} / w_{ii}]} \quad (2)$$

where $\delta_k = \begin{cases} 1 \text{ when } k \text{ is a prompt event} \\ -1 \text{ when } k \text{ is a delayed coincident event} \end{cases}$

IV. Dual (Histogram/List-mode) Reconstruction Scheme

Here we describe a dual (histogram/list-mode) reconstruction scheme to reduce the time cost for dynamic PET imaging, and the criterions which determine the switching point of reconstruction mode should be addressed. One criterion we are currently considering is the number of coincidence events or the size of the data file. For the case of our HRRT scanner, there are 450M LOR's in span 3; therefore, ideally if the number of events in a dynamic frame is less than the number of LOR's (a threshold value of 450M), then one should use the event-based list-mode reconstruction and vice versa given that both reconstruction algorithms are equally optimized. However, in our present implementation OP-LMEM algorithm is not fully optimized, whereas the 3D-OP-OSEM is; as a result, the threshold value in our case is less than the expected 450M. In order for this scheme to work, the quantitative accuracy of the list-mode reconstruction needs to be verified with that of the histogram-mode reconstruction. The comparison schemes are described next.

V. Methods

Tomograph: Data were acquired on the second generation of the High Resolution Research Tomography (HRRT) [8]. This HRRT scanner has an octagonal detector ring design,

with detector heads consisting of a double 10 mm layer of LSO/LYSO for a total of 119,808 detector crystals.

Phantom study: A 20 cm long, 10 cm radius phantom was used. The phantom has three 5 cm diameter cylindrical inserts, one of them was filled with water, another one was Teflon (two 'cold' inserts), and one with a ^{11}C radioactivity concentration of 47 kBq/ml ('hot' insert). The rest of the phantom was filled with a ^{11}C concentration of 11.7 kBq/ml ('background'), giving a hot to background ratio of 4.0. Twenty four dynamic frames (of 360s each) were reconstructed. The measurement thus covered 7 half-lives, and the counts per frame ranged between 2M and 200M.

Comparison schemes: Dynamic images were reconstructed using (i) 3D-OP, (ii) OP-LMEM, and (iii) H-LMEM both with and without the scatter correction in span 3. The following comparisons were performed:

1) Transaxial profile comparisons (with and without the scatter correction): A line profile was placed along a summed transaxial plane (summed over 100 axial planes). The line traverses the hot spot and one of the cold spots (teflon). The transaxial profiles of all 24 frames were compared between the histogram and both list-mode reconstructions with the same number of subsets and iterations (4 iterations with 8 subsets).

2) Axial profile comparisons (with the scatter correction): Mean voxel intensities within each axial plane were plotted as a function of the axial position. The ROI placed covered the whole cross section of the phantom (i.e. including the hot, cold, and background regions). The axial uniformities of all frames were compared between the histogram and both list-mode reconstructions.

3) Contrast, ROI, and voxel noise vs number of iterations comparisons (with the scatter correction): The percent contrast of the cold cylinder (i.e. (1-mean ROI activity of the cold spot over that of the average background)*100%) and the coefficient of variation (for both ROI-level and voxel-level) of the background were calculated for all frames according to the NEMA protocol for different iterations of the OP-LMEM, H-LMEM, and the 3D-OP reconstructions. Contrast and noise were plotted as a function of number of iterations, and comparison was performed between histogram and both list-mode reconstructions.

4) Time activity curve (TAC) comparisons (with the scatter correction): The time activity curve, with the ROI described in 2) on a single plane, was plotted over 24 frames for 3D-OP, OP-LMEM, and H-LMEM reconstructions.

5) Reconstruction time cost comparisons (with the scatter correction): The reconstruction time cost was plotted as a function of the number of counts in each frame and as a function of frame number for both 3D-OP and OP-LMEM reconstructions. In both cases, the same number of computer processors was used. The time costs for the re-binning process and estimating the scatter and random corrections are excluded in the comparison since they are the same for both 3D-OP and OP-LMEM.

VI. Results

The transaxial profiles of frame 10 for histogram (3D-OP) and list-mode (OP-LMEM, H-LMEM) reconstructions are shown in Fig. 2. The axial profiles of frame 10 for the three algorithms are depicted in Fig. 3. Frame 10 was arbitrarily chosen here, and other frames all show similar results.

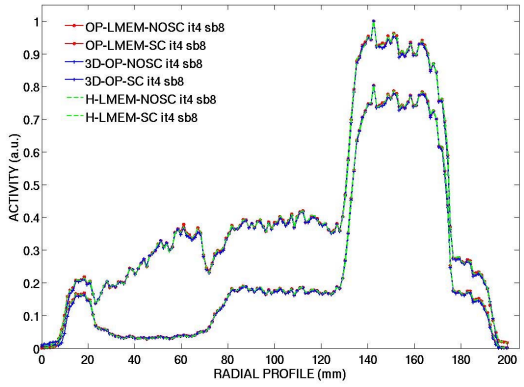

Fig. 2: Transaxial profile comparison for frame 10

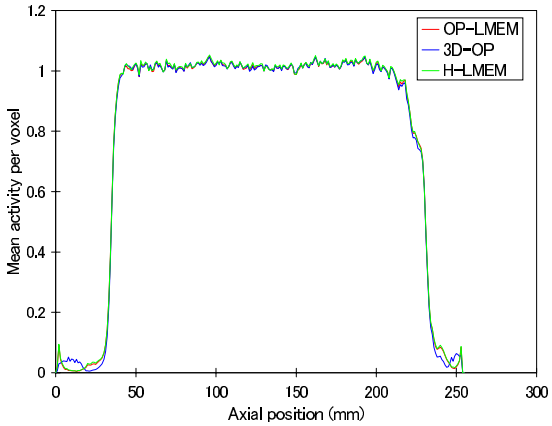

Fig. 3: Axial profile comparison for frame 10

In all cases, the profiles agree very well between 3D-OP, OP-LMEM, and H-LMEM for all 24 frames. The percent contrast, ROI noise, and voxel noise vs number of iterations for frame 10 for all reconstructions are shown in Fig. 4, 5, and 6, respectively.

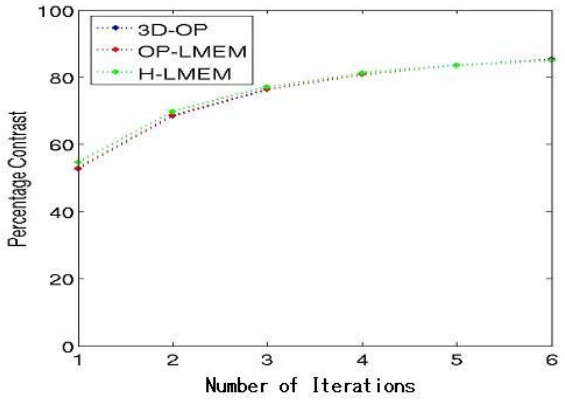

Fig. 4. Contrast vs number of iteration comparison for frame 10

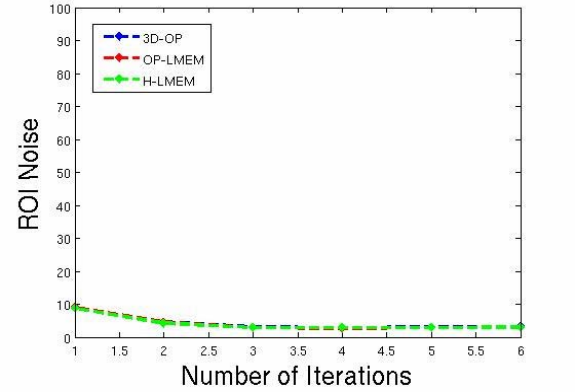

Fig. 5. ROI noise vs number of iteration comparison for frame 10

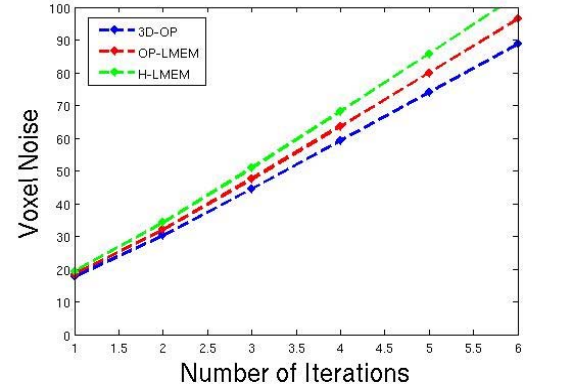

Fig. 6. Voxel noise vs number of iteration comparison for frame 10

Here the contrast also agrees between histogram and list-mode reconstructions with H-LMEM being slightly higher in the first four iterations (i.e. converge slightly faster) as expected since H-LMEM is similar to a sinogram-subtraction precorrection based algorithm with the scatter correction in the denominator of the EM algorithm (see section II) . In addition, the ROI noise comparison shows a good agreement between all three algorithms. The voxel noise shows a slight difference in all three algorithms with the H-LMEM being the highest due to the increased variance in the delay subtraction technique. The difference in noise behaviour between 3D-OP and OP-LMEM is likely due to the difference between a voxel-driven backprojection (3D-OP) and a LOR-driven backprojection (OP-LMEM). As shown in Fig. 7, after applying a 2mm 3D Gaussian filter which we now use to reduce the noise in all our images, the voxel noise for the 3D-OP reconstruction very much agrees with that for the OP-LMEM reconstruction thus minimizing the practical difference between the images reconstructed using both algorithms. In addition, the voxel noise for H-LMEM is still a bit biased after applying the filter as compared to 3D-OP and OP-LMEM.

The TAC's for 3D-OP, OP-LMEM, and H-LMEM are shown in Fig. 8. The counts per frame vary from 2M to 200M.

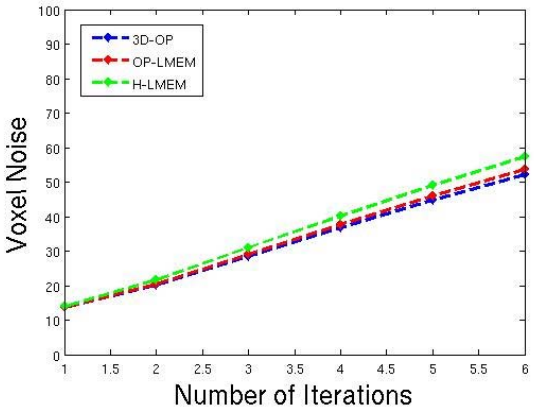

Fig. 7. Voxel noise vs number of iteration comparison after apply a 2mm Gaussian filter

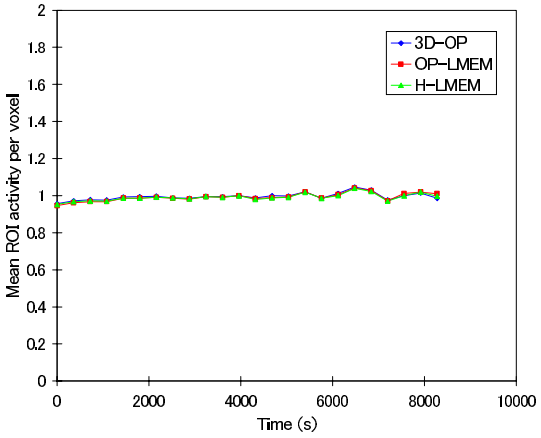

Fig. 8. Time activity curve for 3D-OP, OP-LMEM, and H-LMEM reconstructions

Again, the TAC's agree very well between the histogram-mode and list-mode reconstructions. The reconstruction time cost as a function of number of counts is depicted in Fig. 9.

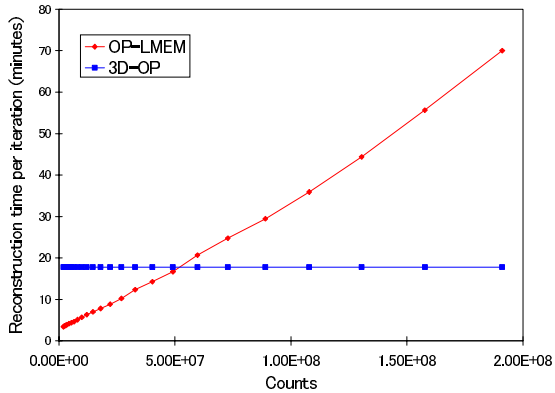

Fig. 9. The reconstruction time cost v.s. the number of counts using the same number of processors for both 3D-OP and OP-LMEM reconstructions

The intercept between the two curves shown in Fig.9 determines the threshold value for the dual reconstruction scheme. Ideally, the threshold value should be the number of LOR's if both OP reconstructions are equally optimized. In

this case, the threshold value of 50M counts was obtained since OP-LMEM is not fully optimized as compared to 3D-OP. The reconstruction time cost is also plotted as a function of frame number in Fig. 10.

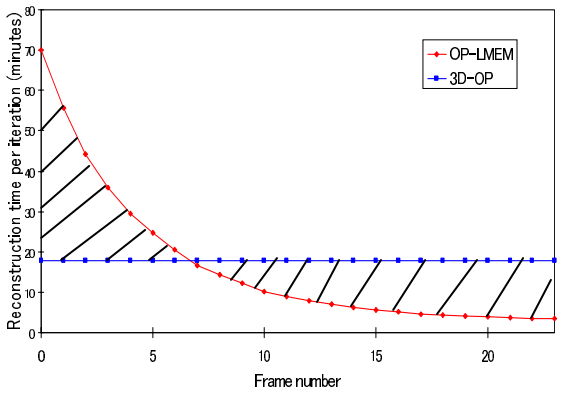

Fig. 10. The reconstruction time cost v.s. the number of counts using the same number of processors for both 3D-OP and OP-LMEM reconstructions

The time we gained by applying the dual reconstruction is basically depicted by the (shaded) area in between the two curves in Fig. 10. It depends on the threshold value, the number of frames, and the number of counts in the frames. In this study, we gained about 40% of time as compared to reconstructing all frames using 3D-OP or OP-LMEM. We will gain even more time once the OP-LMEM is optimized.

VII. Future Work

It has been recently discovered that in a situation where the number of counts changes rapidly within a single frame, the way the time subsets are distributed (see section II) in the list-mode reconstruction will produce visible systematic difference in the image as compared to the histogram-mode reconstruction. This is due to the fact that the later time subsets contain a higher or lower than average number of counts compared to the earlier time subsets in spite of some degree of time interleaving thus introducing a bias. It has been also observed that there are some minor random variations between images reconstructed using 3D-OP and OP-LMEM at low statistics. Random variations were attributed to the fact that although the two methods use the same overall data, the subsets are not identical: in a situation of low counts, statistical differences in the subsets will produce a different reconstructed image. A solution to the systematic bias will be to regroup the list-mode time subset such that the number of counts is uniform or less variant over the subsets, and this is also likely to reduce the random differences between 3D-OP and OP-LMEM. This implementation will be made and tested shortly.

VIII. Conclusion

Preliminary results from phantom studies look excellent. In particular the excellent agreement reached between OP-LMEM and 3D-OP indicates that the implementation of this scatter correction method into the list-mode algorithm is appropriate thus reaching the same level of quantification accuracy as 3D-OP. At present with 3D-OP being fully optimized for speed, while this is not yet the case for our OP-LMEM, we have found that for frames with less than 50M counts OP-LMEM is more advantageous time-wise, and that will set the threshold value for the dual reconstruction scheme to be 50M. By applying the dual reconstruction scheme for the phantom study presented here, we gain about 40% of reconstruction time as compared to reconstructing all frames using 3D-OP or OP-LMEM. In a situation of rapidly changing number of counts within a frame the OP-LMEM was found to produce biased results – a different subset selection scheme is currently under investigation.

In conclusion, we have developed an efficient OP-LMEM algorithm which is equivalent to the histogram-mode counter part, and these studies show a promising feasibility of the dual (histogram/list-mode) reconstruction scheme for the dynamic (4D) studies in PET imaging using the HRRT scanner.

Acknowledgment

The authors would like to especially thank Dr. Kelvin Raywood for his continuous support particularly in regards to facilitation of the group's parallel-computing cluster.

References

[1] A. Rahmim, M. Lenox, A. J. Reader, C. Michel. Z. Burbar, T. J. Ruth, and V. Sossi, "Statistical list-mode image reconstruction for the high resolution research tomography," *Phys. Med. Biol.*, vol. 49, pp. 4239-4258, 2004.

[2] A. Rahmim, J.-C. Cheng, S. Blinder, M-L Camborde, and V. Sossi, "Statistical dynamic image reconstruction in state-of-the-art high resolution PET," Phys. Med. Biol., vol. 50, pp. 4887-4912, 2005.

[3] C. C.Watson, "New, Faster, Image-Based Scatter Correction for 3D PET," *IEEE Trans. Nucl. Sci.* , vol. 47, pp. 1587-1594, 2000.

[4] H. M. Hudson and R. S. Larkin, "Accelerated image reconstruction using ordered subsets of projection data", *IEEE Trans. Med. Imag.*, vol. 13, no. 4, pp. 601-609, 1994.

[5] M. E. Casey and E. J. Hoffman, "Quantitation in positron emission tomography: 7. A technique to reduce noise in accidental concidence meansurements and coincidence efficinecy calibration," *J. Comput. Assist. Tomogr.*, vol. 10, no. 5, pp. 845-850, 1986.

[6] R. D. Badawi, M. P. Miller, D. L. Bailey, and P. K. Marsden, "Randoms variance-reduction in 3D-PET," *Phys. Med. Biol.* vol. 44, pp. 941-954, 1999.

[7] L. Byars, C. Michel *et al.*, to be published, 2005.

[8] K. Wienhard, M. Shmand, M. E. Casey, K. Baker, J. Bao, L. Eriksson, W. F. Jones, C. Knoess, M. Lenox, M. Lercher, P. Luk, C. Michel, J. H. Reed, N. Richerzhagen, J. Treffert, S. Vollmar, J. W. Young, W. D. Heiss, and R. Nutt, "The ECAT HRRT: Performance and First Clinical Application of the New High Resolution Research Tomograph," *IEEE Trans. Nucl. Sci.* vol. 49, pp. 104-110, 2002.